A SIX-YEAR RECORD OF VOLCANIC ASH DETECTION WITH ENVISAT MIPAS

S. Griessbach[1], L. Hoffmann[1], M. von Hobe[2], R. Spang[2], R. Müller[2], and M. Riese[2]

[1]*Jülich Supercomputing Centre (JSC), Forschungszentrum Jülich, 52428 Jülich, Germany, Email:s.griessbach@fz-juelich.de*
[2]*Institut für Energie und Klimaforschung (IEK-7), Forschungszentrum Jülich, 52428 Jülich, Germany*

ABSTRACT

For the Michelson Interferometer for Passive Atmospheric Sounding (MIPAS) on-board ESA's Envisat a fast detection method for volcanic ash was developed that can be applied globally and for long time series. From radiance simulations with the JUelich RApid Spectral SImulation Code (JURASSIC) taking single scattering into account an ash detection threshold was derived based on two spectral windows. This threshold allows to distinguish between ice clouds and small volcanic ash particles with a scattering radius range of $0.4-3.1\,\mu$m. For the eruption of the Chilean Puyehue-Cordon Caulle volcano in June 2011 it is demonstrated that the detection threshold works well in practice. The analysis of MIPAS data with this new ash detection method shows that all major volcanic eruptions were detected between 2006 to 2012.

Key words: MIPAS; volcanic ash; JURASSIC; radiative transfer modelling; Mie scattering.

1. INTRODUCTION

Volcanic ash particles have an impact on the Earth's radiation budget and can pose a severe danger to air traffic. Therefore, the ability to detect and characterise volcanic ash layers on a global and altitude-dependent scale is essential. To obtain a global coverage satellite remote sensing instruments are best suited. For several nadir instruments in the visible and infrared range volcanic ash detection algorithms already exist (see [1] and references therein). However limb sounding instruments provide information on vertical structures in addition. For this reason it is desirable to detect volcanic ash also with limb sounding instruments. In the following we demonstrate that it is possible to detect volcanic ash with an infrared limb sounding instrument.

The instrument best suited for this demonstration is the Michelson Interferometer for Passive Atmospheric Sounding (MIPAS) [2] on-board ESA's Envisat, which is mainly used for measurements of vertical profiles of atmospheric trace gases and temperature, but is also very sensitive to cloud and aerosol particles. MIPAS measures infrared emission spectra between 4.1 to 14.6 μm. In the nominal mode since 2005 the polar orbiting instrument measures 14 orbits per day with approximately 90 profiles per orbit. The altitude coverage is between $6-70$ km in the polar regions and about $11-70$ km in the tropics. The vertical distance between the spectra of a profile is 1.5 km below 20 km altitude and the vertical field of view is 3 km. With MIPAS it is possible to estimate the cloud top height with an accuracy of about 1.5 km [3].

Reference [4] showed with radiance simulations, which include Mie scattering, that Eyjafjallajökull ash particle size distributions, as measured by [5], are detectable with MIPAS and in certain cases are distinguishable from ice clouds using micro windows between $825-830$ and $946-951\,\mathrm{cm}^{-1}$. For these micro windows radiative transfer calculations for different particle types and for different atmospheric conditions and cloud altitudes are performed with the JUelich RApid Spectral Simulation Code (JURASSIC). This allows to define an ash detection threshold to distinguish between ash and ice clouds. In a case study of the eruption of the Chilean volcano Puyehue-Cordon Caulle the viability of this threshold is shown. Finally, six years of MIPAS data are analysed using the new ash detection threshold.

2. SIMULATIONS

2.1. JURASSIC model

The JURASSIC forward model developed by [6] is a spectrally averaging model applying the emissivity growth approximation (EGA) [7, 8, 9] and Curtis Godson approximation (CGA) [10, 11]. To perform fast radiative transfer calculations in the infrared the conventional line-by-line approach is not applied, but spectral mean values of emissivity, Planck function, and radiance are calculated on the spectral grid of any instrument the simulations are intended for. Spectral mean emissivities are obtained by fast interpolation from pre-computed look-up-tables, which are derived from exact line-by-line calculations of the Reference Forward Model (RFM) [12]. JURASSIC has been used for limb and nadir sounding

Proc. of 'ATMOS 2012 – Advances in Atmospheric Science and Applications', Bruges, Belgium (ESA SP-708, November 2012)

remote sensing applications (e.g. CRISTA-NF, MIPAS, AIRS, PREMIER) [13, 14, 15, 16, 17]).

To account for scattering on clouds and aerosol in the infrared radiative transfer, a scattering module was implemented into JURASSIC [4]. For spherical particles Mie scattering is used to calculate the optical properties and for non-spherical ice particles look-up tables of the optical properties e.g. by [18] can be applied.

2.2. Radiance simulations for ice, ash and sulfate particles

As shown by [4] it is possible to distinguish ice cloud spectra from volcanic ash spectra using spectral windows at 825 and 950 cm^{-1}. For this study we chose small windows of less than 1 cm^{-1} width to avoid strong interferences with molecular lines. For these spectral windows we applied JURASSIC taking into account single scattering to calculate the average radiances for a large set of different atmospheric conditions, tangent altitudes, particle concentrations and sizes. The simulated radiances are used to determine radiance thresholds for the detection of volcanic ash.

To cover a wide range of seasonal and latitudinal atmospheric variability we chose the polar winter, polar summer, mid-latitude night, and equatorial standard atmospheres given by [19]. We defined four 1D cloud scenarios with cloud layers of 1 km thickness at 7, 9, 13, and 17 km altitude. For these four cloud scenarios we used the refractive indices of ice [20], volcanic ash [21] and sulfate [22] to simulate ice clouds, ash clouds, and sulfate aerosol layers respectively. For the number size distributions we used log-normal distributions with a width of 1.6 and varied the median radius between $0.01 - 96\,\mu$m. The number concentrations are varied such that the extinction coefficients range from $1{\cdot}10^{-3}$ to 1 km^{-1} for ice, from $1{\cdot}10^{-3}$ to $5{\cdot}10^{-1}$ km^{-1} for ash, and from $1{\cdot}10^{-6}$ to $1{\cdot}10^{-2}$ km^{-1} for sulfate aerosol.

The simulation results are shown in Fig. 1. From the simulations we derived an ash detection threshold (black line). For none of the ice cloud simulations the ash detection threshold was exceeded by the simulated radiances. But for certain particle sizes and extinction coefficients this threshold can be exceeded by ash clouds or sulfate layers. The distinguishable extinction coefficient and scattering radius range for this new detection method are given in Tab. 1. As the plots already indicate, it is not possible to distinguish all ash particles from ice particles. However particle size distributions with a scattering radius up to 3.1 μm can be distinguished from ice clouds. Also for the two largest simulated extinction coefficients of the sulfate aerosol the ash detection threshold can be exceeded. Yet to reach these extinction coefficients either unrealistically high particle concentrations or larger particle sizes than 1.7 μm radius are needed. Simulations with number size distributions measured by [23] after the Pinatubo eruption do not exceed this threshold.

3. OBSERVATIONS

3.1. Puyehue-Cordon Caulle case study

The eruption of the Chilean volcano Puyehue-Cordon Caulle started on 4 June 2011 and emitted particles to altitudes up to 13.7 km [24]. At these high altitudes the jet stream quickly distributed the ash particles around the southern hemisphere. The first ash observations with MIPAS were made on 6 June over the southern Atlantic ocean. On subsequent days the ash was transported eastwards. On 10 June the observed ash particles nearly reached New Zealand. In Fig. 2 the data of a complete orbit, which was measured on 10 June 2011, are shown. In the scatter plot in the left panel the radiances for the two windows at 825 and 950 cm^{-1} are shown for each measured spectrum of that orbit. In the orbit plot in the right panel it is clearly visible that all ash detections cluster together around 40 – 55 S and 100 E.

In Fig. 3 top left panel all profiles measured on 10 June 2011 are denoted with grey dots. For the ash detection the profiles were analysed from high to low altitudes. If there was a cloud indicated by a cloud index smaller than 1.8 [25] the lower altitudes were not analysed. For all profiles with ash detections the highest tangent altitude with an ash signal is colour coded in the map. The relevant volcanoes for June 2011 are indicated by red triangles. The orbit shown in Fig. 2 is located west of Australia.

In the top right panel of Fig. 3 all profiles with ash detections made in the month of June 2011 are shown. Within a month the ash was spread from the Puyehue over the southern hemisphere between about 30 to 80 S. In the Antarctic region there are only few ash detections possible, due to the occurrence of polar stratospheric clouds at higher altitudes. North of 30 S there are also only few detections. This is due to the MIPAS measurement geometry, where in the tropics the lowest MIPAS tangent altitude is above 11 km (Fig. 2 right panel). The ash detections north of 50 N have their origin in the eruption of the Icelandic Grimsvötn volcano, which started on 21 May 2011. Most of the particles were transported northwards. On 13 June 2011 the Eritrean Nabro volcano erupted. Trajectory analysis showed that the particles were first transported north-westwards and later eastwards. The ash detections corresponding to this eruption are located between 25 to 50 N.

The bottom left panel of Fig. 3 shows all profiles with ash detections for July 2011. In the bottom right panel there are all profiles with ash detections for August 2011. In July nearly all ash from the Grimsvötn and Nabro eruptions has disappeared, but a lot of ash from the Puyehue-Cordon Caulle eruption is still left. A few days after the Puyehue-Cordon Caulle eruption the highest particle cloud altitudes of about 12 – 14 km were observed. Later on, the particles are diluted and slowly descend with time. In July the highest ash cloud top altitudes are most frequently observed between 9 – 11 km. In August most particles are left at altitudes between 6 – 8 km. From

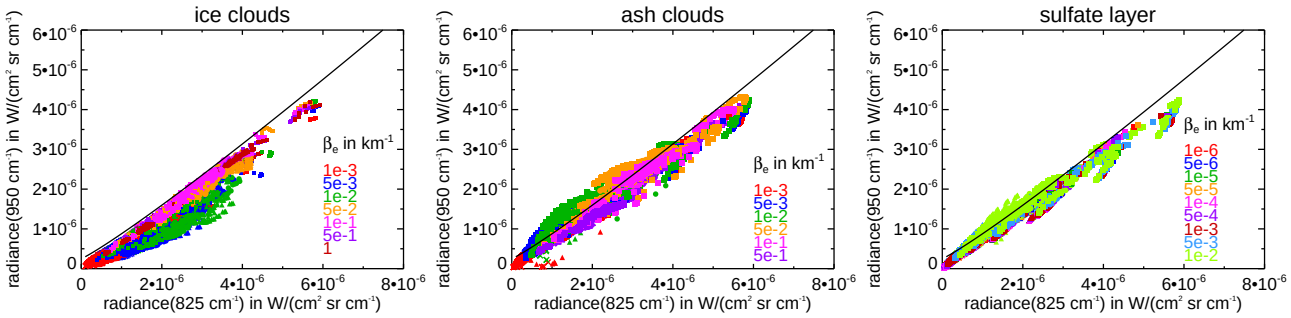

Figure 1. Scatter plots of modelled radiances at 825 and 950 cm^{-1} for different cloud scenarios. The left panel shows all ice cloud scenarios, the middle panel shows all ash cloud scenarios, and the right panel shows all sulfate aerosol scenarios. The black line denotes the ash detection threshold. The extinction coefficients are colour coded. The polar winter atmosphere simulations are denoted by a circle, polar summer by a triangle, mid-latitude by a cross and the tropics by a square.

Table 1. Extinction coefficient ranges and scattering radius ranges that exceeded the ash detection thresholds in the simulations.

particle type	extinction coefficient range in km^{-1}	scattering radius range in μm
volcanic ash	$5{\cdot}10^{-3} - 1{\cdot}10^{-1}$	0.4 – 3.1
sulfate aerosol	$5{\cdot}10^{-3} - 1{\cdot}10^{-2}$	0.4 – 2.8

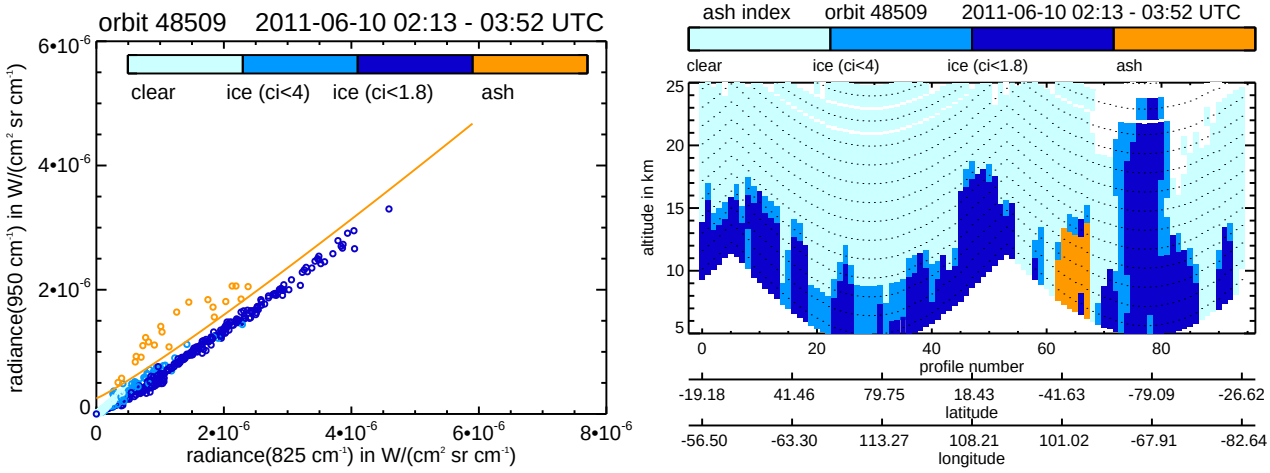

Figure 2. Left: Scatter plot of the radiances of the 825 and 950 cm^{-1} windows for all spectra of MIPAS orbit 48509 measured on 10 June 2011. The orange line denotes the ash detection threshold. Right: Plot of the same orbit showing the location of the vertical profiles of this orbit. Spectra with a cloud index smaller than 1.8 are coloured in dark blue and spectra with the more conservative cloud index of 4 are coloured in middle blue. Clear air spectra are light blue and the ash spectra are highlighted with orange.

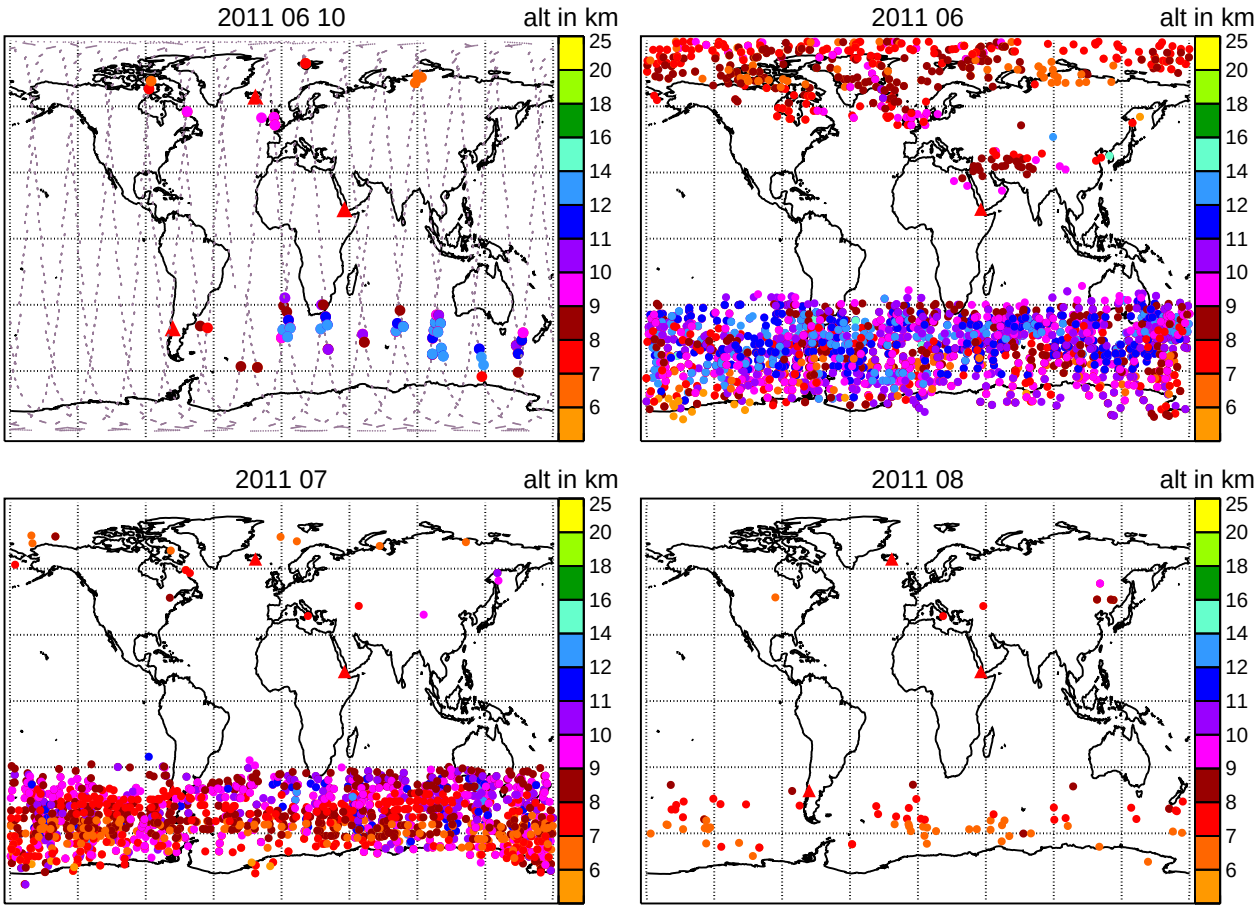

Figure 3. Maps of volcanic ash detections made on 10 June 2011 (top left panel), all detections for the month of June 2011 (top right panel), July 2011 (bottom left panel), and August 2011 (bottom right panel).

Table 2. Number of detections for selected volcanic eruptions and the corresponding relative contribution to overall detections.

Total Number of Detections	5811	100%
After volcanic eruptions	4161	71.6%
Eyafjallajökull	323	5.6%
Karymsky & Grimsvötn	373	6.4%
Okmok & Kasatochi	600	10.3%
Puyehue-Cordon Caulle	1483	25.5%
Redoubt	300	5.2%
Sarychev	855	14.7%
Other significant eruptions	227	3.9%
Wildfires	8	0.1%

these three upper levels a sedimentation speed of about $4.2\,\mathrm{m\,h^{-1}}$ can be estimated. Following [26] and [27] this implies a particle size of about $2-3\,\mu$m. This result is consistent to the simulations of detectable particle sizes and demonstrates that especially small ash particles can be observed for up to three month with IR limb sounding instruments such as MIPAS.

3.2. Six-year statistics of ash detections

We analysed all MIPAS measurements from 2006 to 2011 with our new ash detection method. The results are shown in Fig. 4 as a function of time and latitude. Out of 1.97 million measured profiles the presence of volcanic ash was detected in 5811 profiles, which is about 0.3% of all profiles. To identify the sources of the detected ash we analysed daily ash detection maps and carried out backward trajectory calculations with the Chemical LAgrangian Model of the Stratosphere (CLaMS), which was extended to the troposphere by [28, 29]. As listed in Tab. 2 71.6% of all ash detections could already be attributed to known volcanic eruptions.

The most detections of volcanic ash with MIPAS observed in the last 6 years were caused by the eruptions of the Puyehue-Cordon Caulle in 2011 followed by Sarychev in 2009 and Kasatochi in 2008. In the southern hemisphere, apart from the Puyehue-Cordon Caulle eruption, the Merapi eruption in 2010 and the Chaiten eruption in 2008 were also observed in our data. Furthermore, we found that the ash index also was able to detect severe wildfires such as the Black Saturday Bush Fire in Australia in February 2009 and two other fires in Mozambique/South Africa in 2007 and 2008. For the southern hemisphere we could attribute 98% of the detections to a distinct source.

In the northern hemisphere mainly volcanoes from the northern Pacific Ring of Fire and from Iceland contributed to the ash detections. 62% of all detections we could attribute to eruptions of the Bezimianny, Karymski, Kasatochi, Okmok, Redoubt, Sarychev, Sheveluch, Eyjafjallajökull, Grimsvötn, and Nabro volcanoes.

Obviously there are only few ash detections in the tropics

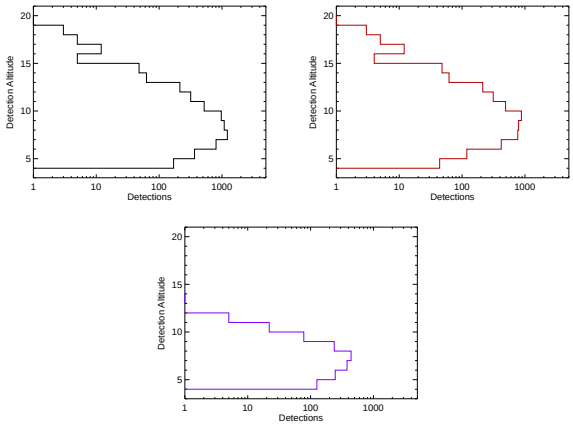

Figure 5. Count statistics of the ash cloud top altitudes. In the top left panel all detections are shown. In the top right panel all the identified detections are shown and in the bottom panel there are the unidentified detections.

between 30°N to 30°S. This is mainly due to the MIPAS measurement geometry. In the tropics the lowest MIPAS tangent altitude is located around 11 km and there were only few volcanic eruptions in the past 6 years that injected volcanic ash particles into altitudes above 11 km. In Fig. 5 count statistics of the observed tangent altitudes of our ash detections are shown. In the left panel there are all detections, in the middle panel the detections we attributed to a distinct event, and in the right panel the unidentified detections. Most ash detections were made in the upper troposphere and lower stratosphere region between 6 to 12 km altitude. It should be noted that the unidentified detections occur in the troposphere at altitudes below 12 km.

4. SUMMARY

We developed a reliable and fast method to detect volcanic particles in the stratosphere and troposphere for infrared limb measurements with MIPAS. Optical properties of volcanic ash, sulfate aerosol, and ice particles, such as extinction coefficients, single scattering albedo, and phase function as well as simulated radiance spectra are used to identify two spectral windows at 825 and $950\,\mathrm{cm^{-1}}$ for the detection of volcanic particles. The calculations were performed with JURASSIC using a newly implemented scattering module.

Our method applies a radiance threshold to distinguish volcanic ash and sulfate aerosol from ice particles. The threshold is derived from simulations of MIPAS radiances with JURASSIC for a broad range of atmospheric conditions and cloud scenarios. From the JURASSIC calculations we conclude that for the scattering radius range between $0.4-3.1\,\mu$m and the aerosol extinction coefficient range from $5{\cdot}10^{-3}-1{\cdot}10^{-1}\,\mathrm{km^{-1}}$ volcanic particle identification is feasible. The simulations also show

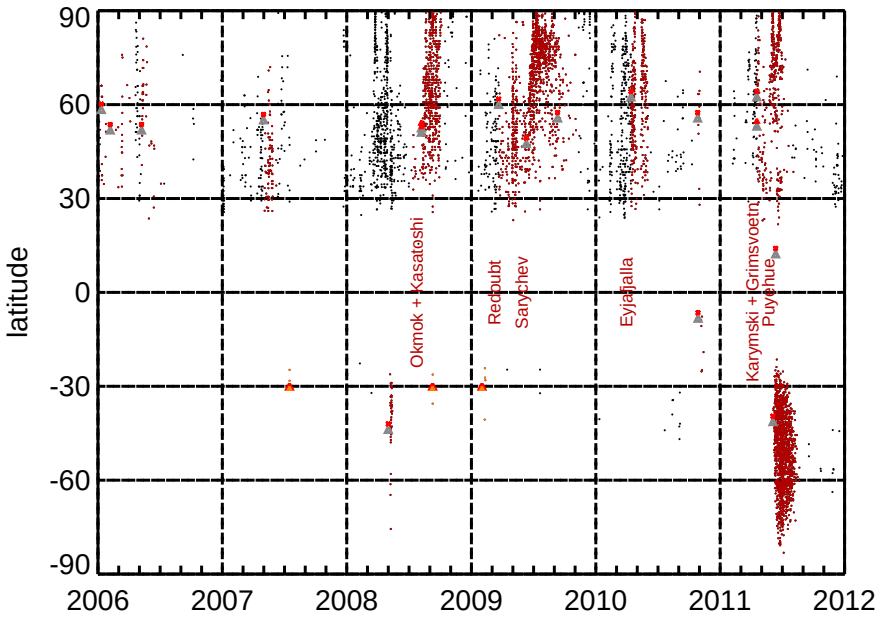

Figure 4. Profiles with volcanic ash detections for 2006 – 2011 depending on latitude. The number of detections for selected volcanoes can be found in Tab. 2

that it might be possible to detect sulfate aerosol as well if either the number concentrations or particles sizes are large. However, from the simulations we found that high concentrations of stratospheric aerosol as measured after the Pinatubo eruption do not exceed the threshold.

The case study of the Puyehue eruption demonstrated the viability of volcanic ash detection with this new method. Ash particles were detected from two days to up to three months after the eruption. This was possible because MIPAS is very sensitive especially to small ash particles. The analysis of the sedimentation speed showed that particles with a scattering radius between $2-3\,\mu$m were detected, which is consistent with the detectable particle range.

The statistical analysis of six years of measured MIPAS radiances confirms the threshold derived from simulations. With this new method major eruptions from e.g. Chaiten, Okmok, Kasatochi, Sarychev, Eyafjallajökull, Merapi, Grimsvötn, Puyehue-Cordon Caulle, Nabro as well as several smaller eruptions at mid-latitudes and in polar regions between 2006 - 2011 were clearly identified in the MIPAS data.

5. OUTLOOK

Especially in the northern hemisphere there are still several unidentified detections. It is likely that not all of them are of volcanic origin. In the southern hemisphere we already identified three severe wildfires among the ash detections. The extinction coefficient spectra of other material, such as carbonaceous aerosol, desert dust, and meteoric dust show a similar spectral slope as volcanic ash between the two spectral windows used in the analysis presented above. With the help of trajectory calculations the work will be continued to localise the potential source regions of the detected events.

ACKNOWLEDGEMENTS

We thank Karlheinz Nogai, Forschungszentrum Jülich, Germany, for technical support. We thank the European Space Agency for providing Envisat MIPAS data.

REFERENCES

[1] C. Zehner, Ed. Monitoring volcanic ash from space. *Proceedings of the ESA-EUMETSAT workshop on the 14 April to 23 May 2010 eruption at the Eyjafjoll volcano, South Iceland.*, Frascati, Italy(26-27 May 2010), 2010. ESA-Publication STM-280.

[2] H. Fischer, M. Birk, C. Blom, B. Carli, M. Carlotti, T. von Clarmann, L. Delbouille, A. Dudhia, D. Ehhalt, M. Endemann, J. M. Flaud, R. Gessner, A. Kleinert, R. Koopman, J. Langen, M. López-Puertas, P. Mosner, H. Nett, H. Oelhaf, G. Perron, J. Remedios, M. Ridolfi, G. Stiller, and R. Zander. MIPAS: an instrument for atmospheric and climate research. *Atmos. Chem. Phys.*, 8:2151–2188, 2008.

[3] R. Spang, J. J. Remedios, L. J. Kramer, L. R. Poole, M. D. Fromm, M. Muller, G. Baumgarten, and P. Konopka. Polar stratospheric cloud observations by MIPAS on Envisat: detection method, validation and analysis of the northern hemisphere winter 2002/2003. *Atmos. Chem. Phys.*, 5:679–692, 2005.

[4] Sabine Griessbach. *Clouds and aerosol in infrared radiative transfer calculations for the analysis of satellite observations*. PhD thesis, Bergische Universität Wuppertal, Germany, 2012. ISBN 978-3-89336-785-6.

[5] U. Schumann, B. Weinzierl, O. Reitebuch, H. Schlager, A. Minikin, C. Forster, R. Baumann, T. Sailer, K. Graf, H. Mannstein, C. Voigt, S. Rahm, R. Simmet, M. Scheibe, M. Lichtenstern, P. Stock, H. Rüba, D. Schäuble, A. Tafferner, M. Rautenhaus, T. Gerz, H. Ziereis, M. Krautstrunk, C. Mallaun, J.-F. Gayet, K. Lieke, K. Kandler, M. Ebert, S. Weinbruch, A. Stohl, J. Gasteiger, S. Groß, V. Freudenthaler, M. Wiegner, A. Ansmann, M. Tesche, H. Olafsson, and K. Sturm. Airborne observations of the Eyjafjalla volcano ash cloud over Europe during air space closure in April and May 2010. *Atmos. Chem. Phys.*, 11(5):2245–2279, 2011.

[6] Lars Hoffmann. *Schnelle Spurengasretrieval für das Satellitenexperiment Envisat MIPAS*. PhD thesis, Bergische Universität Wuppertal, Germany, 2006. ISSN 0944-2952.

[7] Michael P. Weinreb and Arthur C. Neuendorffer. Method to apply homogeneous-path transmittance models to inhomogenous atmospheres. *J. Atmos. Sci.*, 30:662–666, 1973.

[8] Larry L. Gordley and James M. Russell. Rapid inversion of limb radiance data using an emissivity growth approximation. *Appl. Optics*, 20:807–813, 1981.

[9] Benjamin T. Marshall, Larry L. Gordley, and D. Allen Chu. BANDPAK: Algorithms for modeling broadband transmission and radiance. *J. Quant. Spectrosc. Radiat. Transfer*, 52:581–599, 1994.

[10] A. R. Curtis. Discussion of 'A statistical model for water vapour absorption' by R. M. Goody. *Quart. J. Roy. Meteorol. Soc.*, 78:638–640, 1952.

[11] W. L. Godson. The evaluation of infra-red radiative fluxes due to atmospheric water vapour. *Quart. J. Roy. Meteorol. Soc.*, 79:367–379, 1953.

[12] A. Dudhia. *RFM Software User's Manual*. Department of Atmospheric, Oceanic and Planetary Physics, University of Oxford, United Kingdom, 2004. http://www.atm.ox.ac.uk/rfm.

[13] L. Hoffmann, K. Weigel, R. Spang, S. Schroeder, K. Arndt, C. Lehmann, M. Kaufmann, M. Ern, P. Preusse, F. Stroh, and M. Riese. CRISTA-NF measurements of water vapor during the SCOUT-O3 Tropical Aircraft Campaign. *Adv. Space Res.*, 43:74–81, 2009.

[14] K. Weigel, M. Riese, L. Hoffmann, S. Hoefer, C. Kalicinsky, P. Knieling, F. Olschewski, P. Preusse, F. Stroh, R. Spang, and C. M. Volk. CRISTA-NF measurements during the AMMA-SCOUT-O3 aircraft campaign. *Atmos. Meas. Tech.*, 3:1437–1455, 2010.

[15] L. Hoffmann, M. Kaufmann, R. Spang, R. Müller, J. J. Remedios, D. P. Moore, C. M. Volk, T. von Clarmann, and M. Riese. Envisat MIPAS measurements of CFC-11: retrieval, validation, and climatology. *Atmos. Chem. Phys.*, 8:3671–3688, 2008.

[16] L. Hoffmann and M. J. Alexander. Retrieval of stratospheric temperatures from Atmospheric Infrared Sounder radiance measurements for gravity wave studies. *J. Geophys. Res.*, 114(D07105), 2009.

[17] J. Ungermann, L. Hoffmann, P. Preusse, M. Kaufmann, and M. Riese. Tomographic retrieval approach for mesoscale gravity wave observations by the PREMIER Infrared Limb-Sounder. *Atmos. Meas. Tech.*, 3:339–354, 2010.

[18] A. J. Baran. On the scattering and absorption properties of cirrus cloud. *J. Quant. Spectrosc. Radiat. Transfer*, 89(1-4):17–36, 2004.

[19] J. J. Remedios, R. J. Leigh, A. M. Waterfall, D. P. Moore, H. Sembhi, I. Parkes, J. Greenhough, M.P. Chipperfield, and D. Hauglustaine. MIPAS reference atmospheres and comparisons to V4.61/V4.62 MIPAS level 2 geophysical data sets. *Atmos. Chem. Phys. Discuss.*, 7:9973–10017, 2007.

[20] S. G. Warren and R. E. Brandt. Optical constants of ice from the ultraviolet to the microwave: A revised compilation. *J. Geophys. Res.*, 113(D14), 2008.

[21] F. E. Volz. Infrared optical constants of ammonium sulfate, Sahara dust, volcanic pumice and fly ash. *Appl. Optics*, 12:564–568, 1973.

[22] J. R. Hummel, E. P. Shettle, and D. R. Longtin. A new background stratospheric aerosol model for use in atmospheric radiation models. *AFGL-TR-88-0166, Air Force Geophysics Laboratory, Hanscom AFB, MA*, 1988.

[23] T. Deshler, B. J. Johnson, and W. R. Rozier. Balloonborne measurements of Pinatubo aerosol during 1991 and 1992 at 41 degrees n - Vertical profiles, size distribution, and volatility. *Geophys. Res. Lett.*, 20(14):1435–1438, 1993.

[24] Smithonian Global Volcanism Programme, 06 2012. http://www.volcano.si.edu.

[25] R. Spang, J. J. Remedios, and M. P. Barkley. Colour indices for the detection and differentiation of cloud type in infra-red limb emission spectra. *Adv. Space Res.*, 33:1041–1047, 2004.

[26] R. Müller and T. Peter. The numerical modeling of the sedimentation of polar stratospheric cloud particles. *Berichte Der Bunsen-Gesellschaft-physical Chemistry Chemical Physics*, 96(3):353–361, 1992.

[27] Hans R. Pruppacher and James D. Klett. *Microphysics of clouds and precipitation / by Hans R. Pruppacher and James D. Klett*. D. Reidel Pub. Co., Dordrecht, Holland ; Boston :, 1978.

[28] F. Ploeger, L. R. Poole, and L. W. Thomason. Horizontal transport affecting trace gas seasonality in the Tropical Tropopause Layer (TTL). *J. Geophys. Res.*, 117(D09303), 2012.

[29] P. Konopka, J.-U. Grooß, G. Günther, F. Ploeger, R. Pommrich, R. Müller, and N. Livesey. Annual cycle of ozone at and above the tropical tropopause: observations versus simulations with the Chemical Lagrangian Model of the Stratosphere (CLaMS). *Atmos. Chem. Phys.*, 10:121–132, 2010.